JOURNAL OF GEOPHYSICAL RESEARCH, VOL. 92, NO. C9, PAGES 9487-9493, AUGUST 15, 1987

Edge Waves on the Sydney Coast

JASON H. MIDDLETON AND MADELEINE L. CAHILL

School of Mathematics, University of New South Wales, Kensington, Australia

WILLIAM W. HSIEH

Department of Oceanography, University of British Columbia, Vancouver, Canada

Pressure and current oscillations at periods of 40 s to 17 min observed during storm conditions at two locations separated by 560 m in the alongshore direction in the coastal ocean near Sydney, Australia, indicate the existence of infragravity waves having amplitudes of ~20 cm and velocities of ~10 cm s^{-1}. The observed infragravity waves appear to be locally forced by the wind wave envelope through radiation stress, yet the observed alongshore phase differences of the infragravity waves are consistent with those predicted from free edge wave theory for low-mode edge waves travelling northward and the relationship of pressure to velocity at each location is also consistent with free edge wave theory. As a function of time, the infragravity wave spectral energy grows and decays in step with the longer-period wind waves, suggesting a continuous transfer of energy. The infragravity waves appear to contain energy in both directly forced and freely propagating (edge wave) oscillations. The edge waves may be generated either by radiation stress as outlined above, by a resonant triad mechanism, or by a combination of the two.

1. INTRODUCTION

Edge waves are surface gravity waves which are trapped along shore lines by the shoaling topography. They generally have periods somewhat longer than those of wind waves and are believed to play an important role in coastal sedimentation and surf beat [*Bowen and Inman*, 1971; *Huntley and Bowen*, 1975; *Guza and Thornton*, 1985; *Holman and Sallenger*, 1986]. The earliest theory of edge waves appears to be due to *Stokes* [1846], who found wavelike solutions to the barotropic equations of motion appropriate for shallow water on a beach of constant slope. Subsequently, these theories were extended by *Eckart* [1951], *Ursell* [1952], and *Reid* [1958], who identified the discrete modal structure. The dynamics of edge wave propagation are now well understood in principle [*LeBlond and Mysak*, 1978], as is the general relationship of edge waves to the wider class of coastal trapped waves.

Observations of 2- to 30-min-period oscillations in sea level off the California coast led *Munk et al.* [1956] to propose that a "wake" of edge waves of 10- to 30-min period was produced by the impulsive forcing of a moving atmospheric front, while higher frequency waves of 2- to 5-min period were due to surf beat. An extensive alongshore array of pressure gauges was later used on the same beach by *Munk et al.* [1964] to obtain wave number-frequency relations of oscillations with periods of 1 min to 10 hours , and wavelength of 1.5 to 30 km. They concluded that the observed oscillations were predominantly caused by discrete edge wave modes, and that little energy was associated with leaky waves. More recently, *Huntley et al.* [1981] used alongshore and offshore arrays of current meters to show that 1- to 4-min-period oscillations off Scripps beach in California have both structures and dispersion curves consistent with those predicted from edge wave theory.

While the propagation of edge waves is well understood, their generation is not. *Gallagher* [1971], *Guza and Davis* [1974], *Bowen and Guza* [1978] and *Symonds et al.* [1982] argue that nonlinear resonant interactions between incoming surface gravity waves are the main mechanisms for the generation of waves having periods perhaps a few minutes or less. For somewhat longer period waves, *Greenspan* [1956], *Buchwald and de Szoeke* [1973], *Viera and Buchwald* [1982] and *Worthy* [1984] found theoretical solutions for edge waves driven by travelling atmospheric events.

The work reported here was prompted by suggestions by *Buchwald and de Szoeke* [1973] that the 3-min-period oscillations of sea level, observed in Port Kembla harbor (70 km south of Sydney) during storms, were due to storm-generated edge waves travelling northward along the coast. Our experiment was designed as a pilot study to observe the magnitude of oscillations with periods of 0.5 - 17 min in the coastal ocean south of Sydney and to determine if the observed propagation rates are consistent with edge wave theory. Since edge waves propagate because of refraction by shoaling topography, a section of relatively straight coastline with steep cliffs and few energy absorbing inlets was chosen, this occurring off the Royal National Park ~25 km south of Sydney and ~45 km north of Port Kembla (Figure 1).

This paper is organized as follows. Section 2 outlines edge wave theory and experiment design while section 3 describes the experimental method and the observations. A comparison of observation with theory is undertaken in section 4, while section 5 concludes with a discussion.

2. EDGE WAVE THEORY AND DESIGN OF EXPERIMENT

We choose a Cartesian coordinate system with the x axis pointing offshore and the y axis alongshore. The sea level displacement η is assumed to have a travelling wave form, with

$$\eta = F(x)e^{i(ky-\omega t)} \tag{1}$$

From the unforced shallow water equations, the coastal trapped wave equation for linear waves in a barotropic ocean is derived by LeBlond and Mysak [1978, equation (25.7)]. Neglecting the Earth's rotation, we can rewrite their equation as

$$F''-k^2F+H^{-1}(H'F'+\omega^2g^{-1}F)=0 \tag{2}$$

where prime denotes differentiation with respect to x, $H=H(x)$ denotes the depth, and g is the gravitation constant. The eigenvalues of (2), which determine the dispersion relation $\omega=\omega(k)$, and the eigenfunctions $F(x)$ were found numerically

Paper number 7C0393.
0148-0227/87/007C-0393$05.00

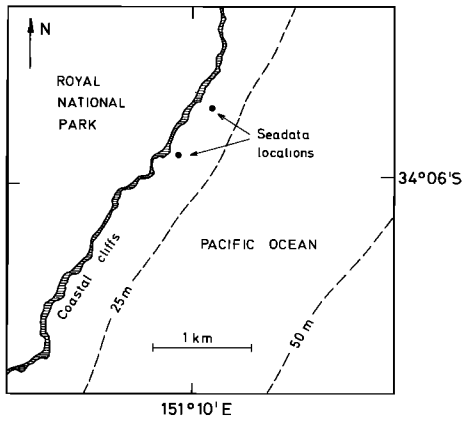

Fig. 1. The coastal region off the Royal National Park, Sydney, Australia, including the locations of the Seadata 635-12S pressure-current recorders used in this study.

[*Holman and Bowen*, 1979] using $F'/F = -(k^2-\omega^2/[gH(L)])^{1/2}$ where $H'(L) = 0$ in the deep ocean $x = L$. Since the coastline at $x = 0$ is composed of cliffs, we also used $H(0) = 10$ m and $F'(0) = 0$.

The depth profile $H(x)$ in our experimental area together with the predicted offshore dependence of the modal structure for 1.3- and 3.3-min waves are shown in Figure 2*a* while the mode 0, 1, and 2 edge wave dispersion curves are shown in Figure 2*b*.

From *LeBlond and Mysak* [1978, equation (25.3) with $f = 0$], one can easily show that the edge wave velocity components obey

$$u = g\omega^{-1}F' \exp\left[i\left(ky - \omega t - \frac{\pi}{2}\right)\right] \quad (3)$$

$$v = gk\omega^{-1}F \exp\left[i(ky - \omega t)\right] \quad (4)$$

and the pressure perturbation p obeys

$$p = \rho g F \exp\left[i(ky - \omega t)\right] \quad (5)$$

where ρ is the water density and (5) follows from $p = \rho g \eta$. Hence v and p are in phase, each leading u by 90°.

The atmospherically forced problem was studied by *Buchwald and de Szoeke* [1973] and *Viera and Buchwald* [1982]. As their depth profiles have a vertical wall at the coast, the edge wave

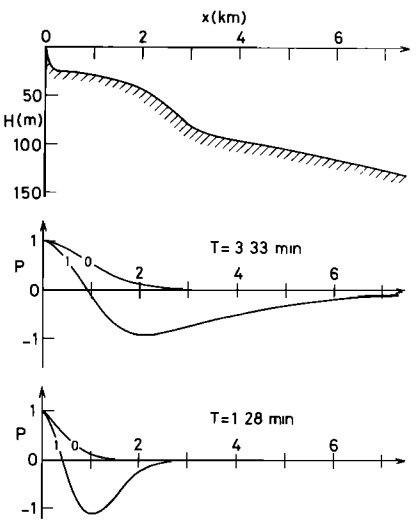

Fig. 2*a*. The offshore depth profile together with the offshore structure of the pressure (sea level) field for the zeroth and first mode edge waves of period 1.28 min and 3.33 min found from the theory.

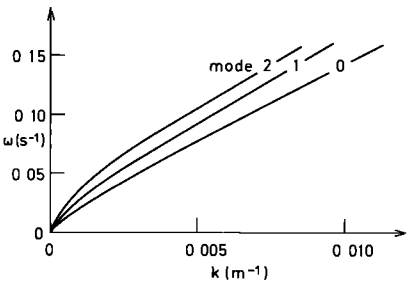

Fig. 2*b*. The dispersion curves for the first three edge wave modes calculated from the theory using the actual depth profile.

phase speed c is confined to $c_{min} < c < c_{max}$, where $c_{min} = [gH(0)]^{1/2}$ and $c_{max} = [gH(L)]^{1/2}$. Depending on the alongshore propagation speed C of the atmospheric front, three situations may occur: (1) $C > c_{max}$, (2) $c_{min} < C < c_{max}$, and (3) $C < c_{min}$. In case 1 the waves generated are not coastally trapped, while in case 3, except for some transients, no wavelike motions are generated. Only in case 2 are edge waves with $c = C$ resonantly excited. For depth profiles with $H = 0$ at the coast, $c_{min} = 0$, and case 3 does not arise. With $H(0) = 10$ m and $H(L) = 5000$ m, we have $c_{min} = 10$ m s^{-1} and $c_{max} = 220$ m s^{-1}.

From our dispersion diagram (Figure 2*b*), the zeroth mode edge wave with c matching the fastest frontal speed C of about 23 m s^{-1} have a period of around 8 min and a wavelength of 12 km. On the other hand, the zeroth mode wave with a 1-min period has a wavelength of 1 km and a phase speed of $c = 17$ m s^{-1}. These spatial and time scales basically determined the instrument locations and the sampling rates.

3. The Experiment and the Observations

For this experiment we were able to obtain two Seadata 635-12S instruments capable of measuring both wave pressures and currents at wind wave periods and longer. These were deployed on bottom-mounted tripods so that the sensors were 1.5 m off the bottom. To resolve wavelengths of ~1 km or longer the instruments were deployed 560 m apart and 100 m from the coastal cliffs in 21 m of water. The sampling strategy was to simultaneously burst sample 512 samples at 2-s intervals (for a duration of 17 min and 4 s) with bursts occurring each 30 min. Wave periods (<4 s) unresolved by the measurements were not expected to seriously alias the data as a result of the depth attenuation of shorter-period waves. During the experimental observation period, only one significant storm occurred, and this storm developed gradually rather than arriving as an easily identifiable front.

A typical burst of storm data comprising pressure p, offshore velocity u, and alongshore velocity v components is shown in Figure 3. Superimposed on the raw time series are low-pass-filtered time series calculated using a discrete Fourier transform filter with frequency domain tapering and a half-power period of 40 s. Wind wave amplitudes are clearly considerable (~1 m) with significant orbital currents for waves with periods of ~8-20 s. The low-passed data show the existence of persistent longer-period (~2-20 min) oscillations of much smaller amplitude (~20 cm) and current (~10 cm s^{-1}). Such low-frequency oscillations are often referred to as infragravity waves. Similar plots were obtained for many other bursts during the storm, and in all cases these lower-frequency oscillations existed. Before the storm, amplitudes were negligible, and as the storm gradually developed, the amplitudes of the lower-frequency oscillations increased at about the same rate as did the wind waves.

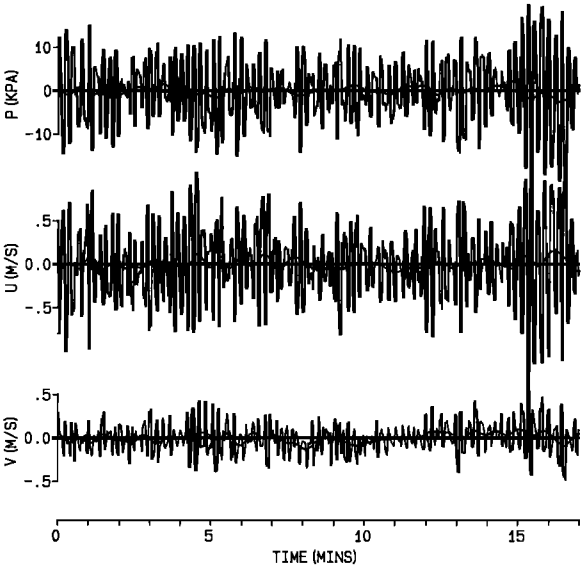

Fig. 3. Time series of pressure p, offshore velocity u and alongshore velocity v for a single burst of 512 samples at 2 second intervals. Overlaid on the raw data are low-passed time series obtained from the raw data using a frequency domain filter with a cosine shaped taper centered at a frequency of 0.025 Hz.

To examine the energy contributions in the frequency domain, spectral estimates for p, u and v were calculated for each burst. To maximise resolution, while maintaining good statistical reliability, the spectral estimates at each frequency were ensemble averaged with those from all other bursts on the same day, giving 96 degrees of freedom. Figure 4 shows spectral estimates from the southern location for the day of maximum wind wave energy. It is clear that in each case, there is significant energy at periods of 5-15 s (wind waves) and that a spectral gap exists at periods of 20-40 s. At periods longer than ~40 s where we observe the

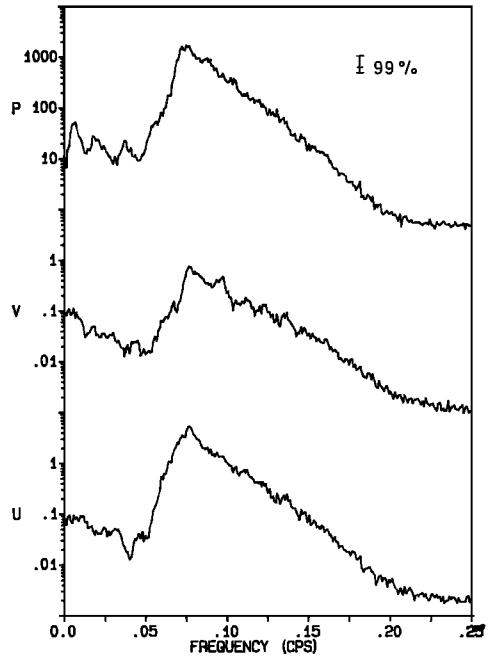

Fig. 4. Spectral estimates of pressure p (kPa^2/cps), Offshore velocity u (m^2 s^{-2}/cps) and alongshore velocity v (m^2 s^{-2}/cps) from the southern Seadata. Each estimate was calculated by ensemble averaging over the spectral and cross-spectral estimates for 48 consecutive bursts, giving 96 degrees of freedom.

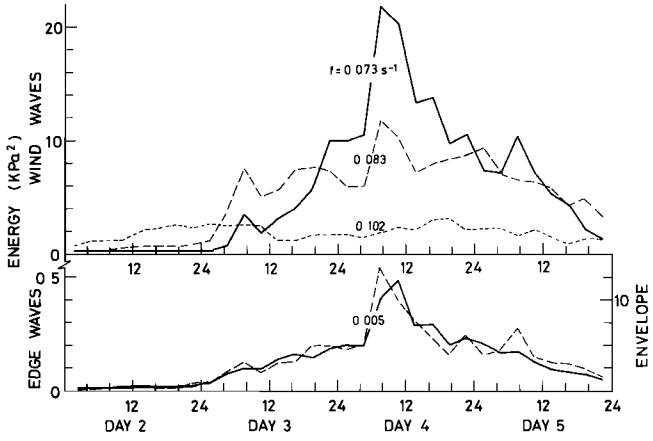

Fig. 5. Spectral estimates $\Phi(f)$ of wind wave, edge wave and envelope series plotted in the form $f\,\Phi(f)$ as a function of time for selected bands centered around the indicated cyclic frequencies f. Wind wave spectra are plotted on the upper axes, while infragravity (solid line) and envelope (dashed line) spectra are shown on the lower axes. Each estimate has 120 degrees of freedom and is plotted using six consecutive bursts of data.

infragravity current and pressure fluctuations in the time series, the spectral estimates rise once more. Although the time series used were not strictly stationary, the spectral distributions of Figure 4 are typical of those found for individual bursts, although the burst spectra were of course substantially noisier.

To investigate the growth of the spectral energies, calculations of spectral estimates as a function of time were made for selected frequency bands. In each case, spectral estimates were obtained by ensemble averaging over 6 bursts (covering 3 hours), and band averaging over 10 adjacent estimates in the frequency domain giving an effective cyclic bandwidth of ~0.01 s^{-1}. The estimates for each consecutive 3-hour period are plotted for the entire storm for the northern Seadata in Figure 5. For the wind wave bands centered on cyclic frequencies of 0.073 s^{-1}, 0.083 s^{-1} and 0.102 s^{-1}, the spectrum for the highest frequency rises first, followed by the spectrum for the next highest frequency. The spectra for the longer-period wind waves rise later, but to larger values. Energy is thus fed to longer and longer period waves as the storm develops, with the high frequency waves (0.102 s^{-1}) approaching some "steady state" value quite early in day 2. The spectral estimates for the infragravity wave band centred at 0.005 s^{-1} include contributions from ~0.001 s^{-1} to 0.010 s^{-1} and thus are essentially estimates of the entire observed infragravity wave spectral energy. Of interest here is the similar shape of the lower-frequency wind wave band and the infragravity wave band; both bands rise and fall in proportion. It therefore seems likely that it is the wind waves of longer period that are feeding energy into the infragravity waves. This linear dependence between the incident longer-period wind wave energy level and the infragravity energy level has been observed by others [e.g., *Tucker*, 1950; *Guza et al.*, 1984], although the data are usually presented by means of significant wave height estimates which mask any frequency dependence. The present spectral calculations show clearly that the infragravity (~200-s period) waves grow linearly only with the longer-period (11-14 s) wind waves, but not with the shorter period (~10 s) waves.

To further investigate the relationship between wind waves and infragravity waves, the pressure time series were band passed to retain cyclic frequencies between 0.065 and 0.095 s^{-1}. Envelope time series for the band-passed data were then found using the method outlined by *Bracewell* [1978] and *Melville* [1983]. Figure

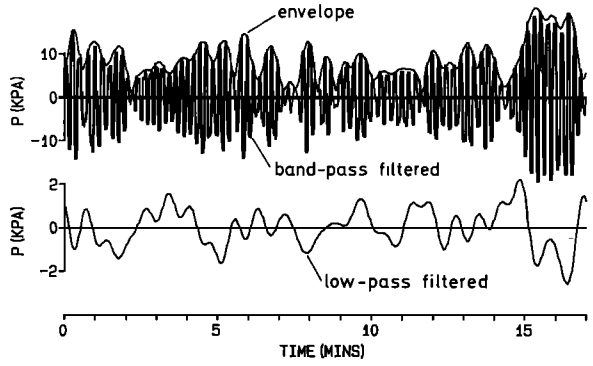

Fig. 6. The band-passed ($0.065 < f < 0.095$ s^{-1}) time series of Figure 3 presented as a carrier frequency of $f = 0.08$ s^{-1} modulated with an envelope function on the upper axes, with the low-passed infragravity time series shown below.

6 shows the band-passed time series from Figure 3 together with the envelope function plotted on the upper set of axes. For visual comparison the low-passed infragravity wave pressure time series for the same burst is shown on the lower set of axes. The wind wave envelope has significant low-frequency energy, and there is some visual correlation between the envelope and the infragravity wave time series. Similar calculations of the spectral energy of the envelope time series were made as a function of time for a frequency band centered on $f = 0.005$ s^{-1} and these are presented in the lower section of Figure 5 for direct comparison with the infragravity wave results. The envelope spectra (dashed line) grow simultaneously with both the longer-period wind wave spectra and the infragravity wave spectra (solid line), indicating that wind wave energy is transferred to the infragravity wave frequencies through the wind wave envelopes. This conclusion is reinforced by calculations summarized by Figure 7, which shows spectral energies, coherences, gain and phase lag between time series of wind wave envelopes and the observed time series at infragravity wave frequencies. Here spectral and cross-spectral estimates have been ensemble averaged over the 48 bursts of day 4. Spectral energies for the envelope series are larger than those for the infragravity wave time series by a factor of 20; however, as is shown by the gain (wherein only the coherent contributions are compared), there is approximately 10% as much coherent energy in the infragravity wave spectrum as in the envelope spectrum. Coherences are significant over much of the plotted

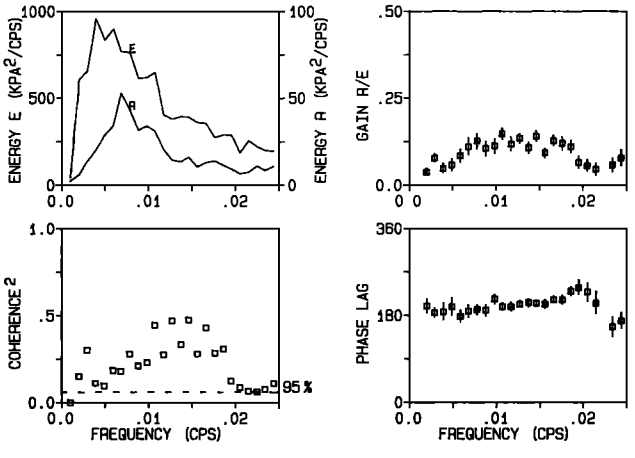

Fig. 7. Spectral and cross-spectral quantities of the pressure envelope time series (E) and the observed time series (R) at infragravity frequencies, ensemble averaged over 48 bursts.

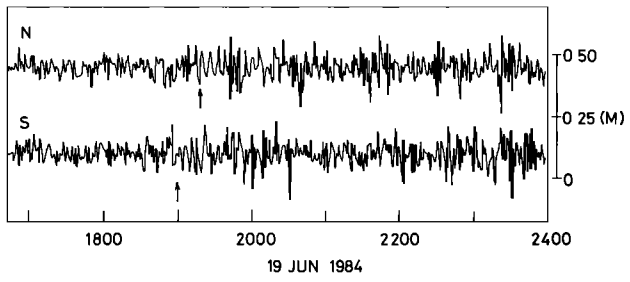

Fig. 8. Time series of sea level found from the pressures recorded by two Aanderaa pressure gauges separated by 10 km in the alongshore direction. The characteristic oscillations beginning at ~1900 LT in the southern (S) data and ~1920 LT in the northern (N) data are associated with the passage of a strong front on June 19.

range, while there appears to be a phase lag of $\sim\pi$. *Longuet-Higgins and Stewart* [1962, 1964] coined the term "radiation stress" for the nonisotropic flow of momentum due to the presence of water waves. They showed theoretically that groups of waves having large amplitudes have a high radiation stress which causes an expulsion of fluid below, thus leading to a reduced mean sea level. High wave envelopes are therefore π out of phase with variations in the mean sea level. This feature is clearly evident in the present data, indicating that a substantial amount of energy in the observed low-frequency oscillations is locally forced by the wind wave envelope.

As explained earlier, for the particular storm observed with the Seadatas, the wind stress grew gradually, thus preventing any study of the impulsive generation mechanism. Some weeks earlier, however, two Aanderaa pressure gauges were deployed in the same region with a 10-km separation during the passage of a strong front. This front arrived in the Sydney region at about 2000 LT on June 19. Calculations of the speed of the front from Bureau of Meteorology mean sea level atmospheric pressure data suggest an average front speed of ~8 m s^{-1}. Time series of sea level data are shown in Figure 8. Oscillations looking remarkably like the Cauchy-Poisson oscillations depicted by *Lamb* [1932, article 238], and observed by *Munk et al.* [1956] are evident at ~1900 LT (southern gauge) and ~1920 LT (northern gauge). The time lag between the oscillations suggests an apparent speed of propagation of ~8 m s^{-1}, consistent with the speed of the front, and it therefore seems likely that the oscillations are indeed Cauchy-Poisson oscillations caused by the impulse due to the moving front.

Calculation of the phase speeds of lower-mode edge waves shows their speed (>17 m s^{-1}) to be much larger than the front speed. Thus it is unlikely that the resonant mechanisms proposed by *Buchwald and de Szoeke* [1973] and *Viera and Buchwald* [1982] would be effective in this case.

4. Comparison of Observations with Edge-Wave Theory

One method of comparing the infragravity data with theories of edge wave propagation is to measure coherence and phase between time series of observations separated along the direction of propagation. Values of coherence squared and phase were calculated for day 4 of the storm (June 30), this particular day being chosen because the storm and the infragravity wave spectra were largest. The spectral and cross-spectral estimates for pressure and velocity time series were ensemble averaged over all bursts taken on the day, and values of coherence squared and phase are shown in Figure 9. All values of coherence squared are plotted, while plotting of phases was restricted to those points where the coherence squared exceeded the 95% confidence limit

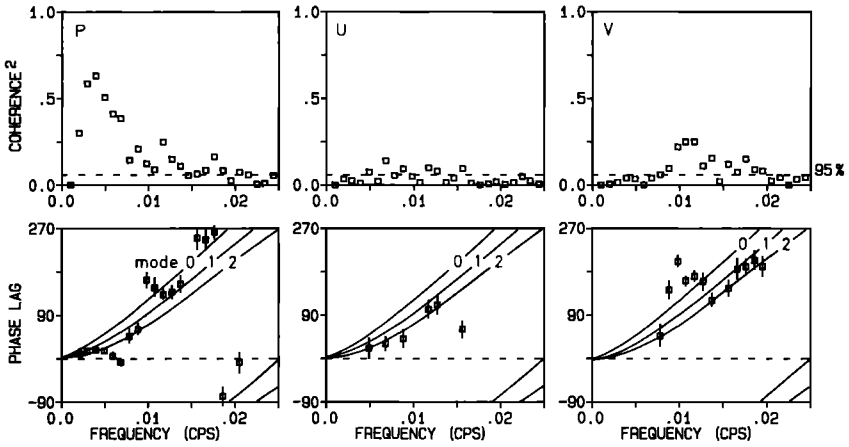

Fig. 9. Coherence squared and coherence phase plotted as a function of frequency for the pressure time series, the offshore velocity time series, and the alongshore velocty time series. The point estimates are found from the data, while the solid lines indicate phase lags predicted for northward propagation of edge waves by the theory.

for the null hypothesis. The nonstationary nature of the time series is less important for calculations of phase which are not expected to be dependent on the energy levels.

There are several noteworthy features. Observed coherences between the pressure time series are significant over most of the range of periods (1-17 min). The observed phase lags (point estimates) show a general increase with increasing frequency, indicating a northward propagation. Predicted phase lags (solid lines) from the theory for the first three edge wave modes are also plotted for comparison. The observations are in general agreement with the theory over most of the frequency range plotted, although the scatter in the observations precludes a precise determination of which modes are responsible.

The offshore and alongshore velocity coherence squared and phase calculations are somewhat different. Coherences are very much lower than those for the pressure series, probably as a result of the current signals being more easily affected by local topographic irregularities. Phases are also somewhat noisy but are reasonably consistent with the theoretical predictions.

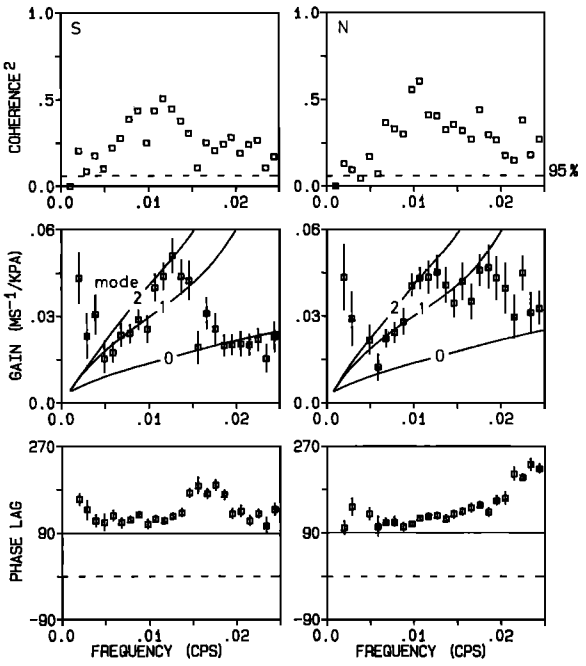

Fig. 10. Estimates of coherence squared, coherence phase, and gain for the pressure and offshore velocity components for each of the Seadata records. Solid lines in the phase and gain plots are found from the theory while the point estimates are found from the data.

There appear to be no phase estimates suggesting a southward propagating wave, so we conclude that the majority of the observed low frequency energy lies in northward propagating infragravity waves, with propagation rates being consistent with edge wave theory.

Another way of examining the properties of the oscillations is to compare the relative amplitudes and phases of the pressure data and the onshore-offshore velocity field as a function of frequency. These calculations were made from the data using a frequency response type of analysis, wherein only the coherent contributions at any frequency are considered. The results predicted by theory for the gain and phase (solid lines) are compared against the estimates obtained from the data (point estimates) in Figure 10 for both the northern and southern Seadatas. In each case the observed phase lags are a little larger than the value of 90% predicted by edge wave theory and this may be due to the orientation chosen for the alongshore (and hence offshore) direction. The orientation of the coastline was chosen to be 035°T, however as was outlined earlier, local small-scale topographic variations might play an important role in "steering" the currents. Estimates of the gain also show good general quantitative agreement with that predicted by edge wave theory, although again there appears to be substantial noise.

In both the plots for the northern and southern data, there are frequency bands where both the gain and the phase appear anomalous. These might be due to the related class of "leaky" edge-waves or to reflected infragravity waves whose energy propagates but is not confined to the modal structure, nor to propagating along the coastal waveguide.

In general, however, these pressure-velocity results show that the observed infragravity oscillations have properties fully consistent with unforced edge wave theory.

5. Discussion

Observations of pressure and velocity made in the coastal ocean off the Royal National Park south of Sydney, Australia, show that infragravity waves with height of ~20 cm and velocity of ~10 cm s^{-1} exist at periods of 40 s to 17 min during storm events. These infragravity waves are apparently locally forced by the radiation stress associated with the incident wind wave envelope, yet the alongshore propagation speeds and the

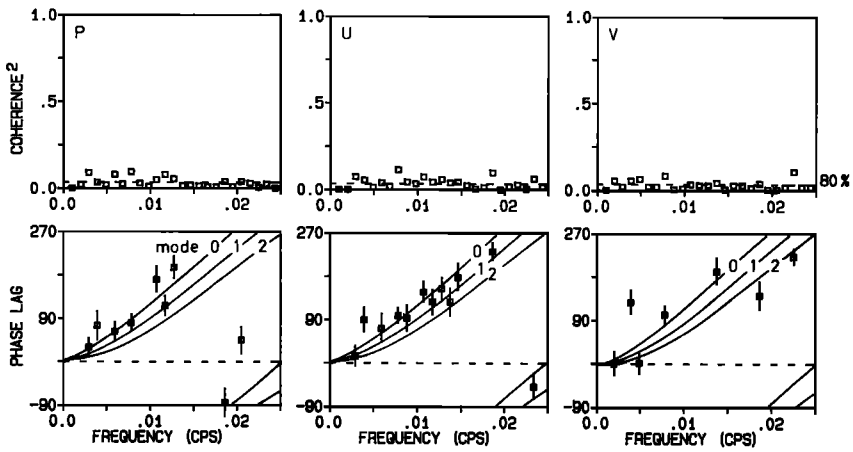

Fig. 11. As for Fig. 9, except that calculations are made for the envelopes rather than the time series.

pressure-velocity relationships are consistent with those predicted from unforced linear edge wave theory. These ideas seem somewhat contradictory; however, from earlier calculations it was found that values of coherence squared for the envelope and infragravity time series (Figure 7) are generally significant but less than 0.5, as are values for the southern and northern infragravity time series (Figure 10). Thus an explanation for the apparent contradiction is that the observed infragravity waves most probably comprise of both locally forced and freely propagating (edge wave) oscillations. The separation of forced and free infragravity oscillations and the identification of the forcing mechanisms have proved elusive in other studies even where the instrument arrays are large, and we do not believe that these issues can be properly addressed with the present data set. Some discussion of possible forcing mechanisms is, however, appropriate.

One possible mechanism is a resonant matching of alongshore propagation speeds of envelopes and edge waves. To investigate this mechanism, coherence and phase estimates were calculated for envelope time series from the southern and northern Seadatas, and these are plotted as points in Figure 11. Superimposed on the phase diagram are the predicted phases for the first three edge wave modes (solid lines), and the general agreement confirms the matching of envelope and edge wave speeds. Coherences are generally lower than for the infragravity time series calculations (Figure 9), adding further weight to the contention that some of the energy resides in natural oscillation (edge waves). Estimates of envelope speeds are readily found in the following way. Calculations of the direction of the incident wind waves as measured by the instruments indicate that the waves propagate basically from the south to southeast quadrant. Wave envelopes approaching the coastline, which has an orientation of ~035°-215°T, will propagate along the coastline at a phase (and group) velocity of $c/\sin\alpha$. Here c is the phase speed of the shallow water waves, and α is the angle between the incident waves and the normal to the coastline as measured by the Seadatas. For the present case where the coastal depth is ~20 m, $c \approx 13$ m s^{-1}, α = 5°-20°, and the apparent speed of propagation of the envelopes along the coast is 35-150 m s^{-1}, overlapping the range of speeds of free edge waves of zeroth mode (17-32 m s^{-1}), first mode (29-68 m s^{-1}), and second mode (38-192 m s^{-1}) at periods of 3.3 to 17 min.

The concept of forcing by resonant triads, proposed by *Bowen and Guza* [1978] and supported by laboratory experiments, predicts resonant forcing at a phase speed of $g(2\omega_0 \sin\alpha_0)^{-1}$, where ω_0 is the central wind wave frequency and α_0 is the angle of incidence in deep water. Knowing the angle of incidence at the point of observation, α_0 may be found by assuming conservation of alongshore wave number as the wind waves shoal. For the present case where $\omega_0 \approx 0.44$-0.56 s^{-1} (corresponding to wave periods of 11-14 s^{-1}), $\alpha_0 \approx 10°$-$30°$, and the range of speed of the forcing is $\approx$ 17-64 m s^{-1}, again quite consistent with the range of speeds for the lower-mode edge waves.

The edge wave spectral energies are observed to develop and decay with time through a storm in step with the longer-period (~14 s) wind waves, suggesting a continuing energy transfer, through possibly one or both of the resonant mechanisms outlined above. The majority of energy appears to be transferred via these mechanisms rather than through an impulsive generation mechanism, although this experiment was not a good test for the impulsive generation theory or for *Worthy*'s [1984] theory of wind-generated edge waves which is practically applicable to waves of period longer than 15 min.

There are several important factors which need consideration, given that a relatively energetic infragravity wave signal exists in the Sydney coastal region. First, harbor resonance is liable to be a continuing problem for harbors such as Port Kembla where the first mode seiching period (~3 min) occurs at periods for which infragravity waves are active. Second, standing edge waves produced by reflection from headlands may provide a generation mechanism or a transport mechanism for the large submerged sand beds which exist further north in the Sydney area [*Gordon and Hoffman*, 1985]. These sand beds exist at 30- to 40-m depth, corresponding to distances offshore of 1-3 km. As is indicated in Figure 2, the edge wave structure is such that for periods of ~3 min or longer, significant edge wave currents will exist as far as 4.5 km offshore. At a 3-min period the mode 0 wavelength is approximately 3.2 km long, a length scale comparable with the observed sand beds.

Acknowledgements. This work was supported by Marine Sciences and Technologies grant 83/1176. We thank Greg Nippard and David Griffin for their mooring expertise, Steedman Ltd for the provision of one Seadata 635-12s and for reading the data tapes, and John Biddlecombe and Dave Adams for the use of M.V. *Laura-E* and M.V. *Elizabeth*, respectively. Bob Guza, Graham Symonds, and the anonymous reviewers provided helpful comments on an earlier draft.

REFERENCES

Bowen, A. J., and D. L. Inman, Edge waves and crescentic bars, *J. Geophys. Res.*, *76*, 8662-8671, 1971.

Bowen, A. J., and R. T. Guza, Edge waves and surf beat. *J. Geophys. Res., 83*, 1913-1920, 1978.

Bracewell, R. N., *The Fourier Transform and its Applications*, 2nd ed, McGraw-Hill, New York, 1978.

Buchwald, V. T., and R. A. de Szoeke, The response of a continental shelf to travelling pressure disturbances, *Aust. J. Mar. Freshwater Res., 24*, 143-158, 1973.

Eckart, C., Surface waves on water of variable depth, *Wave Rep. 100*, 99 pp., Scripps Inst. of Oceanogr., Univ. of Calif., La Jolla, 1951.

Gallagher, B., Generation of surf beat by non-linear wave interactions, *J. Fluid Mech., 49*, 1-20, 1971.

Gordon, A. D., and J. G. Hoffman, Sediment features and processes of the Sydney continental shelf, *Tech. Memo 85/2*, 37 pp., N.S.W. Public Works Dep. Coastal Branch, Sydney, 1985.

Greenspan, H. P., The generation of edge waves by moving pressure distributions, *J. Fluid Mech., 1*, 574-592, 1956.

Guza, R. T., and A. J. Bowen, The resonant instabilities of long waves obliquely incident on a beach, *J. Geophys. Res., 80*, 4529-4534, 1975.

Guza, R. T., and R. E. Davis, Excitation of edge waves by waves incident on a beach, *J. Geophys. Res., 79*, 1285-1291, 1974.

Guza, R. T., and E. B. Thornton, Observations of surf beat, *J. Geophys. Res., 90*, 3161-3172, 1985.

Guza, R. T., E. B. Thornton and R.A. Holman, Swash on steep and shallow beaches, in *Proceedings of the Nineteenth Coastal Engineering Conference*, ASCE, Vol 1, edited by B.L. Edge, pp. 709-723, American Society of Civil Engineers, 1984.

Holman, R. A., and A. J. Bowen, Edge waves on complex beach profiles, *J. Geophys. Res., 84*, 6339-6346, 1979.

Holman, R. A., and A. H. Sallenger Jr., High-energy nearshore processes, Eos Trans. AGU, 67(49), 1369-1371, 1986.

Huntley, D. A., and A. J. Bowen, Field observations of edge waves and their effect on beach material, *J. Geol. Soc. London, 131*, 68-81, 1975.

Huntley, D. A., R. T. Guza and E. B. Thornton. Field observations of surf beat, 1, Progressive edge waves, *J. Geophys. Res., 86*, 6451-6466, 1981.

Lamb, H. L., *Hydrodynamics*, 6th ed., Dover, New York, 1932.

LeBlond, P. H., and L. A. Mysak, *Waves in the Ocean*, Elsevier, New York, 1978.

Longuet-Higgins, M. S., and R. W. Stewart, Radiation stress and mass transport in gravity waves, with application to "surf-beats," *J. Fluid Mech., 13*, 481-504,1962.

Longuet-Higgins, M. S., and R. W. Stewart. Radiation stresses in water waves: A physical discussion, *Deep-Sea Res., 11*, 529-562, 1964.

Melville, W. K., Wave modulation and breakdown, *J. Fluid Mech., 128*, 489-506, 1983.

Munk, W., F. Snodgrass, and G. Carrier, Edge waves on the continental shelf, *Science, 123*, 127-132, 1956.

Munk, W., F. Snodgrass, and F. Gilbert, Long waves on the continental shelf: An experiment to separate trapped and leaky modes, *J. Fluid Mech., 20*, 529-554, 1964.

Reid, R. O., Effect of Coriolis force on edge waves, I, Investigation of the normal modes, *J. Mar. Res., 16(2)*, 24-33, 1958.

Stokes, G. G., Report on recent researches in hydrodynamics, Rep. 16th Meet. Brit. Assoc. Adv. Sci., Southampton, 1846, Murray, London, pp. 1-20, 1846.

Symonds, G., D. A. Huntley, and A. J. Bowen, Two dimensional surf beat: Long wave generation by a time varying breakpoint, *J. Geophys. Res., 87*, 492-498, 1982.

Tucker, M. J., Surf beats: Sea waves of 1 to 5 min. period, *Proc. R. Soc. London, Ser. A, 202*, 565-573, 1970.

Ursell, F., Edge waves on a sloping beach, *Proc. R. Soc. London, Ser. A, 214* ,79-97, 1952.

Viera, F., and V. T. Buchwald, The response of the east Australian continental shelf to a travelling pressure disturbance, *Geophys. Astrophys. Fluid Dyn., 19*, 249-265, 1982.

Worthy, A. L., Wind-generated, high-frequency edge waves, *Aust. J. Mar. Freshwater Res., 35*, 1-7, 1984.

M. L. Cahill and J. H. Middleton, School of Mathematics, University of New South Wales, Kensington, N. S. W., Australia, 2033.

W. W. Hsieh, Department of Oceanography, University of British Columbia, Vancouver, B. C., Canada V6T 1W5.

(Recieved September 16, 1986;
revised April 12, 1987;
accepted April 13, 1987.)